

ment as observed on Venus [5,6]. Such a process accounts for the long run-out flows consistently originating downrange in oblique impacts (i.e., opposite the missing ejecta sector) even if uphill from the crater rim. Atmospheric turbulence and recovery winds decoupled from the gradient-controlled basal run-out flow continues downrange and produces wind streaks in the lee of topographic highs. Turbulence accompanying the basal density flows may also produce wind streak patterns. Uprange the atmosphere is drawn in behind the fireball (and enhanced by the impinging impactor wake), resulting in strong winds that will last at least as long as the time for crater formation (i.e., minutes). Such winds can entrain and saltate surface materials as observed in laboratory experiments [2,3] and inferred from large transverse dunes uprange on Venus [2].

**Atmospheric Effects on Ballistic Ejecta:** Even on Venus, target debris will be ballistically ejected and form a conical ejecta curtain until its outward advance is decelerated by the atmosphere. The well-defined, radial ejecta delineating the uprange missing ejecta sector of craters formed by oblique impacts demonstrate ballistic control of ejection. As the inclined ejecta curtain advances outward, however, it creates turbulent vortices, which have been observed in the laboratory experiments [2] and modeled theoretically [7]. The ejecta curtain gradually becomes more vertical in response to atmospheric resistance. The atmospheric density is sufficient to decelerate meter-sized ejecta to terminal velocities [8] that will be entrained in and driven by response winds induced by the outward-moving curtain. While larger ejecta are deposited, smaller size fractions become entrained in an outward ejecta flow. Based on diversion of such flows by low-relief barriers near the rims of craters, the transition from ballistic to nonballistic emplacement occurs within about 0.5 crater radii of the rim. This observation underscores the fact that dynamic atmospheric pressure significantly restricts outward advance of the ejecta curtain. The scaled run-out distance (distance from the crater rim scaled to crater diameter,  $D$ ) of the ejecta flow should decrease on Venus as  $D^{-0.5}$ , unless consumed by crater rim collapse. Because of the high atmospheric density, collapse of near-rim ejecta into a flow crudely resembles an avalanche comprised of coarse debris and blocks. But high winds and turbulence created by the outward-moving curtain separate during terminal emplacement of the inner flow, thereby winnowing the finer fractions and creating an overrunning turbidity flow that continues outward.

Turbidity flows containing finer fractions can extend to much larger distances until turbulence supporting entrained debris no longer can support the load. Because turbulent wind velocities greatly exceed ambient surface winds, such vortices are also capable of mobilizing surface materials. It is suggested that the radar-dark lobes extending beyond the inner radar-bright ejecta [2,6] reflect this process. In addition, many craters are surrounded by a very diffuse boundary that masks low-relief ridges and fractures; this boundary may indicate the limits of a third stage of flow separation and deposition. The observed radar-dark signature requires such ejecta to be less than a few centimeters. In contrast with the coarse, radar-bright inner facies, the outer radar-dark facies will be more susceptible to later erosion by ambient or other impact-generated winds because the size fractions were sorted by a similar process. This is consistent with observed removal or reworking of craters believed to be old, based on superposed tectonic features.

**Late Recovery Winds (Secondary Effects of Atmospheric Turbulence):** On planets without atmospheres, the effects of early, high-speed ejecta and impactor are typically lost. On Venus, however, the dense atmosphere not only contains this energy fraction, but the long recovery time of the atmosphere (Fig. 1b)

results in late-stage reworking, if not self-destruction, of ejecta facies emplaced earlier. Surface expression should include bedforms (e.g., meter-scale dunes and decimeter-scale ripples) reflecting eddies created in the boundary layer at the surface. Because radar imaging indicates small-scale surface roughness (as well as resolved surface features), regions affected by such long-lived low-energy processes can extend to enormous distances. Such areas are not directly related to ejecta emplacement but reflect the atmospheric equivalent to distant seismic waves in the target. Late-stage atmospheric processes also include interactions with upper-level winds. Deflection of the winds around the advancing/expanding fireball creates a parabolic-shaped interface aloft. This is preserved in the fall-out of finer debris for impacts directed into the winds aloft (from the west) but self-destructs if the impact is directed with the wind. Exception to this rule occurs for larger crater (>60 km) sufficient to interrupt the flow pattern not only by the fireball but also by the ejecta curtain.

**References:** [1] Schultz P. H. and Gault D. E. (1990) In *GSA Spec. Pap.* 247 (V. L. Sharpton and P. D. Ward, eds.), 239–261. [2] Schultz P. H. (1992) *JGR*, in press. [3] Schultz P. H. (1992) *JGR*, in press. [4] Ivanov B. A. et al. (1986) *Proc. LPSC 16th*, in *JGR*, 91, D413–D430. [5] Schultz P. H. (1991) *Eos*, 73, 288. [6] Phillips R. J. et al. (1991) *Science*, 252, 288–296. [7] Barnouin O. and Schultz P. H. (1992) *LPSC XXIII*, 65–66. [8] Schultz P. H. and Gault D. E. (1979) *JGR*, 84, 7669–7687. [9] Schultz P. H. et al. (1981) In *Multi-Ring Basins, Proc. LPS 12A* (P. H. Schultz et al., eds.), 181–195, Pergamon, New York. [10] Barnouin O. and Schultz P. H. (1992) *LPSC XXIII*, 65–66. [11] Schultz P. H., this volume. [12] Jones E. M. and Sanford M. T. II (1982) In *GSA Spec. Pap.* 190 (L. Silver and P. Schultz, eds.), 175–186. [13] Schultz P. H. (1992) *JGR*, in press. [14] Schultz P. H. and Gault D. E. (1982) In *GSA Spec. Pap.* 190 (L. Silver and P. Schultz, eds.), 153–174. [15] Post R. L. (1974) *AFWL-TR-74-51*.

**N93-14373**

**MAGELLAN PROJECT PROGRESS REPORT.** J. F. Scott, D. G. Griffith, J. M. Gunn, R. G. Piereson, J. M. Stewart, A. M. Tavormina, and T. W. Thompson, Jet Propulsion Laboratory, California Institute of Technology, Pasadena CA 91109, USA.

The Magellan spacecraft was placed into orbit around Venus on August 10, 1990 and started radar data acquisition on September 15, 1990. Since then, Magellan has completed mapping over 2.75 rotations of the planet (as of mid-July 1992). Synthetic aperture radar (SAR), altimetry, and radiometry observations have covered 84% of the surface during the first mission cycle from mid-September 1990 through mid-May 1991.

Operations in the second mission cycle from mid-May 1991 through mid-January 1992 emphasized filling the larger gaps (the south polar region and a superior conjunction) from that first cycle. An Orbit Trim Maneuver (OTM) was performed at the beginning of cycle 2 in order to interleave altimeter footprints at periapsis. This yielded better altimetric sampling of the equatorial regions of Venus. Some 94% of the planet was mapped at the end of mission cycle 2.

Observations in the third mission cycle from mid-January to mid-September 1992 emphasized reimagining of areas covered in cycle 1 and cycle 2 such that digital stereo and digital terrain data products can be produced. A transponder anomaly in January 1992 (just before mission cycle 3 started) forced the project to use a radar data downlink of 115 Kbs instead of 268 Kbs. Although data acquisition is curtailed, some 30–40% of the planet will be mapped

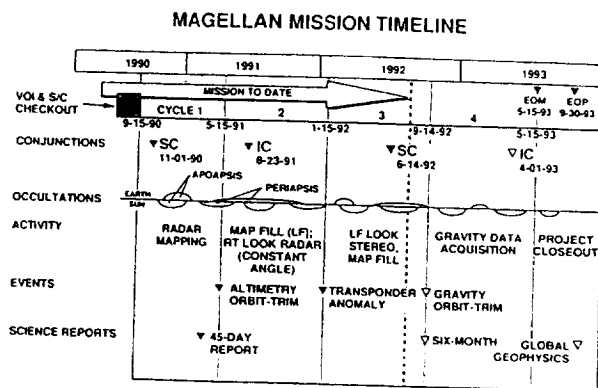


Fig. 1.

in cycle 3. Some 98% of the planet will be mapped at the end of mission cycle 3.

Planned observations in the fourth mission cycle from mid-September 1992 through mid-May 1993 will emphasize high-resolution gravity observations of the equatorial regions of Venus. A second Orbit Trim Maneuver (OTM) at the beginning of this mission cycle will lower periapsis to below 200 km to improve the gravity resolution. Magellan, with its large antenna and X-band radio system, will also improve upon the venusian gravity maps obtained from the Pioneer-Venus spacecraft. These new gravity observations when coupled with superb radar images will provide valuable insights to the interior processes occurring on Venus.

Scientific reports for the project include the "45 Day Report," which was published as a single issue of *Science* in March 1991. A "6-Month Report" will also be published as a special issue of the *Journal of Geophysical Research (JGR) Planets* in the summer of 1992. A "Geophysics Report" on the 360° of gravity observation in cycle 4 will be one or more scientific articles submitted for publication in the summer or fall of 1993.

Magellan data products, the SAR images, altimetry data and radiometry data, are available as analog photographs and digital compact disks (CD-ROMs) at the National Space Science Data Center (NSSDC) at the NASA Goddard Space Flight Center (GSFC) in Greenbelt, Maryland. As of May 1, 1992, over 500 radar mosaics, as well as the altimetry and radiometry data for the first mission cycle, are available. In addition, some 250 photographs have been released and are available to the public. The altimetry and radiometry data for cycle 1 produced by the Massachusetts Institute of Technology (MIT), as well as the cartographic products produced by the U.S. Geological Survey (USGS), are being released to the science community.

## N93-14374

**ATLA REGIO, VENUS: GEOLOGY AND ORIGIN OF A MAJOR EQUATORIAL VOLCANIC RISE.** D. A. Senske and J. W. Head, Department of Geological Sciences, Box 1846, Brown University, Providence RI 02912, USA.

**Introduction:** Regional volcanic rises form a major part of the highlands in the equatorial region of Venus. These broad domical uplands, 1000 to 3000 km across, contain centers of volcanism forming large edifices, and are associated with extension and rifting. Two classes of rises are observed: (1) those that are dominated by tectonism, acting as major centers for converging rifts such as Beta Regio and Atla Regio, and are termed tectonic junctions [1]; and (2) those forming uplands characterized primarily by large-

scale volcanism forming edifices, Western Eistla Regio and Bell Regio, where zones of extension and rifting are less developed. Within this second class of features the edifices are typically found at the end of a single rift, or are associated with a linear belt of deformation [1,2]. In this paper, we examine the geologic characteristics of the tectonic junction at Atla Regio, concentrating on documenting the styles of volcanism and assessing mechanisms for the formation of regional topography.

**Topographic and Geologic Characteristics of Atla Regio:** Atla Regio is a 1000-km × 1000-km highland centered near 4°N, 200° and is a broad rise reaching an elevation of 3.0 km (all elevations are referenced to a planetary radius of 6051.0 km) (Fig. 1). The relationship between chasmata (rifts) and volcanic features forms a pattern similar to that observed at Beta Regio, distinguishing Atla as a major tectonic junction [3,4,5]. In addition, Pioneer Venus gravity data show this highland to have a substantial gravity anomaly, centered at Ozza Mons, along with a corresponding large apparent depth of isostatic compensation (>200 km) [6,7]. Interpretations from these data suggest that like Beta Regio, Atla Regio is most likely a site of mantle upwelling.

Magellan altimetry data provide the first detailed coverage of the topography of Atla Regio (Fig. 1). The regional rise has gentle slopes (0.1° to 0.2°), reaching its highest point at Ozza Mons, a 7.5-km-high peak. In plan view the central part of the highland is triangular shaped with its apex pointing to the north where it intersects the north-south-trending rift valley Ganis Chasma. The legs of the triangle correspond to Dali Chasma (southwest/northeast orientation) and Parga Chasma (southeast/northwest orientation). The more distal parts of all three rifts curve, are aligned along a more east-west orientation, and form a "pinwheel" pattern centered on Ozza Mons. At a point just to the south of where Dali Chasma intersects Ozza Mons a second volcano, Maat Mons, is located on the western edge of the rift and rises to an elevation of 9.2 km. To the northwest of central Atla is a second gentle topographic rise (elevation of 2.0 km) on which is located Sapas Mons, a 4.0-km-high volcano that has a substantial gravity anomaly (+25 mgal at a spacecraft altitude of 200 km) (8). The presence of broad domical topography, the large gravity anomaly, and the presence of large-scale volcanism suggests that Sapas is the site of second thermal anomaly.

**Regional Geology of Atla Regio:** In order to understand the relationships between regional tectonism and volcanism, we examine the geology of the central part of the Atla, concentrating on Ozza Mons and Maat Mons. Geologic mapping of this area (Fig. 2) shows it to contain five general units, the most abundant of which are radar-dark plains. Plains to the northwest of Ozza Mons contain pervasive sinuous ridges (spacing of 10 to 25 km) with a general orientation of N 30°E, parallel to the trend of Ganis Chasma, and are interpreted to be compressional in origin [5]. These structures may have formed by the relaxation of topography or may represent surface deformation linked to large-scale flow in the mantle [5]. To the north of Ozza Mons the plains are disrupted by faulting and fracturing forming a 150- to 250-km-wide rift, Ganis Chasma. Features mapped as edifices correspond to the volcanos Sapas Mons, Maat Mons, and Ozza Montes. An additional volcanic center with a corresponding large gravity anomaly (+35 mgal) is located on the southwest edge of Ganis Chasma (15°N, 195°). This region is located along a chain of gravity highs stretching the length of Ganis Chasma. Lava flows from the volcanic center lie on the edge of the rift, being deposited to the southwest, apparently down the rift flanks and do not appear to contribute to any rift infilling. A number of isolated regions of